The Astrophysical Journal Letters, 989:L18 (10pp), 2025 August 10 https://doi.org/10.3847/2041-8213/adf196

Discovery of an [Fe/H] ~ -4.8 Star in Gaia XP Spectra*

Guilherme Limberg[1], Vinicius M. Placco[2], Alexander P. Ji[1,3], Yupeng Yao[4], Anirudh Chiti[1,3], Mohammad K. Mardini[5,6,7], Anna Frebel[7,8,9], and Silvia Rossi[10]
[1] Kavli Institute for Cosmological Physics, University of Chicago, 5640 S. Ellis Avenue, Chicago, IL 60637, USA; limberg@uchicago.edu
[2] NSF NOIRLab, Tucson, AZ 85719, USA
[3] Department of Astronomy & Astrophysics, University of Chicago, 5640 S. Ellis Avenue, Chicago, IL 60637, USA
[4] Department of Computer Science and Engineering, University of North Texas, 3940 N. Elm Street, Denton, TX 76207, USA
[5] Department of Physics, Zarqa University, Zarqa 13110, Jordan
[6] Jordanian Astronomical Virtual Observatory, Zarqa University, Zarqa 13110, Jordan
[7] Joint Institute for Nuclear Astrophysics–Center for the Evolution of the Elements (JINA-CEE), USA
[8] Department of Physics, Massachusetts Institute of Technology, 77 Massachusetts Avenue, Cambridge, MA 02139, USA
[9] Kavli Institute for Astrophysics and Space Research, Massachusetts Institute of Technology, 77 Massachusetts Avenue, Cambridge, MA 02139, USA
[10] Universidade de São Paulo, Instituto de Astronomia, Geofísica e Ciências Atmosféricas, Departamento de Astronomia, SP 05508-090, São Paulo, Brazil
Received 2025 June 30; revised 2025 July 11; accepted 2025 July 12; published 2025 August 8

Abstract

We report on the discovery of GDR3_526285 (Gaia DR3 Source ID 5262850721755411072), a star with [Fe/H] $= -4.82 \pm 0.25$ and one of the lowest metal (atomic number > 2) mass fractions ever found ($Z_{\rm GDR3-526585} \lesssim 1.0 \times 10^{-6}$). We first identified it as an ultra-metal-poor (UMP; [Fe/H] < -4) red-giant branch (RGB) star candidate in the Gaia Blue (BP) and Red (RP) Photometer (XP) spectrophotometric catalog (Gaia G magnitude ≈ 15). A combination of multiband photometry and high-resolution spectroscopic analysis under local thermodynamic equilibrium confirmed the status of GDR3_526285 as a distant ($\approx$24 kpc from the Sun) RGB star ($T_{\rm eff} = 4596$ K, $\log g = 0.88$) in the Milky Way's outer halo. We obtain only an upper limit for the carbon abundance of [C/H] < -4.32, resulting in [C/Fe] $< +0.50$. A correction for the evolutionary carbon depletion (Δ[C/Fe] $= +0.68$) brings the nominal carbon-to-iron ratio upper limit to $[{\rm C/Fe}]_{\rm cor} < +1.18$. Given its extraordinarily low [C/H], GDR3_526285 likely formed from gas cooled via dust grains rather than fine structure line cooling. The kinematics of GDR3_526285 suggests that this star was either dynamically perturbed by the infall of the Magellanic system or was formerly a member of the Magellanic Clouds and was later stripped by the Milky Way. Our results showcase the potential of an all-sky search for low-metallicity targets with Gaia XP and confirm that the methodology described here is a useful "treasure map" for finding additional UMP stars.

Unified Astronomy Thesaurus concepts: High resolution spectroscopy (2096); Chemical abundances (224); Population II stars (1284); Population III stars (1285); Metallicity (1031); Halo stars (699); Gaia (2360)

1. Introduction

With the realization that "weak-lined" stars are characterized by high-velocity dispersion (N. G. Roman 1950), many programs have searched in the Milky Way's halo for the lowest-metallicity stars (T. C. Beers & N. Christlieb 2005). These metal-poor stars are surviving witnesses to the earliest episodes of chemical enrichment, which are inaccessible through other probes (A. Frebel & J. E. Norris 2015). Specifically, the so-called "ultra-metal-poor" (UMP) stars ([Fe/H] < -4)[11] are presumed to be direct descendants of the first (Population III) stars, and their chemical abundances should preserve the yields of the first metal-free supernovae (e.g., M. N. Ishigaki et al. 2018). For comparison, even with very high-redshift data from JWST (out to $z \sim 10$), measured metallicities in directly observed galaxies rarely reach 1/100th the solar level (e.g., M. Curti et al. 2024), highlighting the key importance of local UMP stars in the Galactic halo. However, being able to study the high-z Universe in detail with nearby UMP stars comes with the challenge that these are extremely rare, with less than 50 such objects known to this day (e.g., P. Bonifacio et al. 2025).

The most prominent feature of Galactic metal-poor stars (here assumed to have [Fe/H] $\lesssim -2$) is that they are typically quite enhanced in carbon relative to iron ([C/H] $-$ [Fe/H] $=$ [C/Fe] $\gtrsim +0.7$; W. Aoki et al. 2007). S. Rossi et al. (1999) first recognized that the fraction of these carbon-enhanced metal-poor (CEMP) stars increases with decreasing metallicity. Indeed, nearly all stars with [Fe/H] $\leqslant -4.5$ are of the carbon-enhanced kind (V. M. Placco et al. 2014; A. Arentsen et al. 2022). For example, the most iron-deficient star known, SMSS J031300.36−670839.3, (with [Fe/H] < -7; S. C. Keller et al. 2014) has an immense carbon-to-iron ratio ([C/Fe] $> +4.5$).

For quite some time, the only potential exception to this behavior has been the UMP star discovered by E. Caffau et al. (2011), SDSS J102915+172927, with [Fe/H] $= -4.73$ and an upper limit of [C/Fe] $< +0.91$ (E. Caffau et al. 2024). This carbon-abundance limit is much lower than that of other stars at the same metallicity, and it leaves room for SDSS J102915 +172927 to potentially not be a CEMP star. Consequently, and given reasonable assumptions about the nitrogen and oxygen abundances (see E. Caffau et al. 2011), its total metal mass fraction is $\sim$10$\times$ lower than that of SMSS J031300.36

* Based on observations gathered with the 6.5 m Magellan Telescopes located at Las Campanas Observatory, Chile.
[11] $[{\rm X/H}] = \log_{10}(N_{\rm X}/N_{\rm H})_\star - \log_{10}(N_{\rm X}/N_{\rm H})_\odot$ for a given star $\star$ and element X.

−670839.3 (S. C. Keller et al. 2014). Recently, additional plausible non-CEMP UMP stars have been discovered both in the Milky Way (E. Starkenburg et al. 2018; V. M. Placco et al. 2021a) and its satellites (Á. Skúladóttir et al. 2021; A. Chiti et al. 2024). These discoveries point to the chemical diversity of UMP stars and, hence, the heterogeneity in the properties of the first stars and supernovae themselves (e.g., A. Heger & S. E. Woosley 2010).

Clearly, identifying additional UMP stars is paramount to the quest to constrain the properties of the first supernovae. Current surveys are now optimized to discover the most metal-poor stars by using narrowband photometry around metallicity-sensitive features of stellar spectra, notably the Ca II K and H lines at $\lambda = 3933$ Å and $\lambda = 3969$ Å, respectively. Then, high-resolution spectroscopy ($\mathcal{R} \gtrsim 20k$) can be used to confirm the metallicities of the candidates and/or derive detailed elemental abundances. Some of these initiatives include the Pristine survey (E. Starkenburg et al. 2017 and D. S. Aguado et al. 2019 for follow-up), the Southern Photometric Local Universe Survey (C. Mendes de Oliveira et al. 2019; see also D. D. Whitten et al. 2021; V. M. Placco et al. 2022; H. D. Perottoni et al. 2024), and the Javalambre Photometric Local Universe Survey (A. J. Cenarro et al. 2019; D. D. Whitten et al. 2019; C. A. Galarza et al. 2022). The newest addition to this list is the Mapping the Ancient Galaxy in CaHK (MAGIC) survey (F. O. Barbosa et al. 2025; A. Chiti et al. 2025, in preparation; V. M. Placco et al. 2025).

The success of the abovementioned narrowband photometric metallicity technique relies on imaging large areas of the sky to efficiently search for these rare low-metallicity stars. In this Letter, we showcase the power of an all-sky search based on the Gaia mission's (Gaia Collaboration et al. 2016) spectrophotometric data with the discovery of a UMP star with one of the lowest iron abundances ever measured ($[\mathrm{Fe/H}] = -4.82 \pm 0.25$) and only an upper limit of carbon ($[\mathrm{C/Fe}]_{\mathrm{cor}} < +1.18$). These properties make Gaia DR3 5262850721755411072 (Gaia Collaboration et al. 2023), hereafter "GDR3_526285," one of the most metal-poor stars ever found.

2. Data

2.1. Target Selection

We identified the UMP star GDR3_526285 in the Gaia mission's third data release (DR3) of Blue (BP) and Red (RP) Photometer (XP) low-resolution spectra ($\mathcal{R} \approx 50$; F. De Angeli et al. 2023; Gaia Collaboration et al. 2023). For the task, we utilize the Gaia XP-based catalog of candidate very metal-poor stars ($[\mathrm{Fe/H}] < -2$) from Y. Yao et al. (2024) as the starting point. These authors constructed an `XGBoost` machine learning classification model (T. Chen & C. Guestrin 2016 for the algorithm) to flag likely low-metallicity stars in Gaia XP. We specifically explore their golden sample of ≈70,000 vetted red-giant branch (RGB) stars with effective temperatures (T_{eff}) and surface gravity values ($\log g$) ideal for the search for stars with very weak absorption lines. To ensure that our UMP candidates were genuine RGB stars, we checked the stellar parameters from R. Andrae et al. (2023; also a data-driven method with Gaia XP) before spectroscopic follow-up.

To narrow our selection of the most promising UMP candidates, we trained an `XGBoost` regression model to predict metallicities for the golden sample of low-metallicity RGB stars from Y. Yao et al. (2024) based on Gaia XP. For the training, we use the compilation of metallicities from high-resolution ($\mathcal{R} \geqslant 15k$) spectroscopic results available in either Stellar Abundances for Galactic Archaeology (SAGA) database or JINAbase (T. Suda et al. 2008; A. Abohalima & A. Frebel 2018)[12] totaling >1200 stars. We combine our metallicity estimates with those from other methods in the literature, including the aforementioned R. Andrae et al. (2023) as well as an internal catalog of XP metallicities (M. K. Mardini et al. 2025, in preparation) that has previously been used to identify a UMP star in the Milky Way's disk (M. K. Mardini et al. 2024) and another in the Large Magellanic Cloud (LMC; A. Chiti et al. 2024).

We selected GDR3_526285 for high-resolution spectroscopic follow-up due to its reddish color indicative of it being a cool star (Gaia $BP - RP = 1.44$), with RGB-like stellar parameters in R. Andrae et al. (2023; $T_{\mathrm{eff}} = 4742$ K and $\log g = 1.38$) and very low predicted metallicity from our regression model ($[\mathrm{Fe/H}]_{\mathrm{XP,Yao+23}} = -3.5$). Our low-metallicity value based on Gaia XP was corroborated by both the R. Andrae et al. (2023; $[\mathrm{Fe/H}]_{\mathrm{Andrae+23}} = -2.9$) and M. K. Mardini et al. (2025, in preparation; $[\mathrm{Fe/H}]_{\mathrm{CaHK}} < -2.9$) catalogs. Lastly, GDR3_526285 is bright enough (Gaia BP = 15.6) to be observed with high-resolution spectroscopy on a 6–8 m class telescope with reasonable exposure times that would allow us to detect absorption features of several different elements.

2.2. Observations

We obtained a high-resolution spectrum of GDR3_526285 on 2023 May 13 with the Magellan Inamori Kyocera Echelle (MIKE; R. Bernstein et al. 2003) instrument attached to the Magellan Clay 6.5 m telescope located at Las Campanas Observatory, Chile. We gathered two exposures of 20 minutes each using a 0.″7 slit and 2 × 2 CCD binning, yielding a resolving power of $\mathcal{R} \sim 35k$ and $28k$ at the blue (wavelength $\lambda < 5000$ Å) and red ($\lambda > 5000$ Å) arms, respectively. The data were reduced with the standard MIKE-specific `CarPy` package (D. D. Kelson 2003).[13] The final 1D spectrum reached signal-to-noise ratio (S/N) ≈ 20 per pixel at $\lambda = 4000$ Å and ≈64 per pixel at $\lambda = 6500$ Å. Regions of interest in the MIKE spectrum are shown in the left panel of Figure 1, namely Ca II K and H at $3920 \lesssim \lambda/\text{Å} \lesssim 3980$ (red) and CH G band at ∼4300 Å (blue). Also shown is a medium-resolution ($\mathcal{R} \sim 1500$) spectrum of GDR3_526285 obtained with the Gemini (South) Multi-Object Spectrograph (GMOS) instrument (R. L. Davies et al. 1997; G. Gimeno et al. 2016) at the Gemini South 8.1 m telescope, which shows a weak Ca K line and no visible CH absorption.[14]

With the reduced data at hand, we derive a line-of-sight velocity (v_{los}) for GDR3_526285 by cross-correlating against a high-S/N MIKE spectrum of metal-poor standard HD122563 ($[\mathrm{Fe/H}] = -2.75$; I. Karovicova et al. 2020) using the

[12] Exact training data for the `XGBoost` regression model: R. Cayrel et al. (2004), J. G. Cohen et al. (2013), I. U. Roederer et al. (2014), H. R. Jacobson et al. (2015), E. M. Holmbeck et al. (2020), and H. Li et al. (2022).

[13] https://code.obs.carnegiescience.edu/mike

[14] We recovered the GMOS spectrum from the Gemini Observatory Archive (https://archive.gemini.edu/); program ID GS-2023B-Q-107, PI: G. Limberg. Two 750 s exposures were obtained with the B600 l mm^{-1} (G5323) grating and a 1.″5 slit and 2 × 2 spatial binning. We perform data reduction with the `DRAGONS` package (K. Labrie et al. 2023).

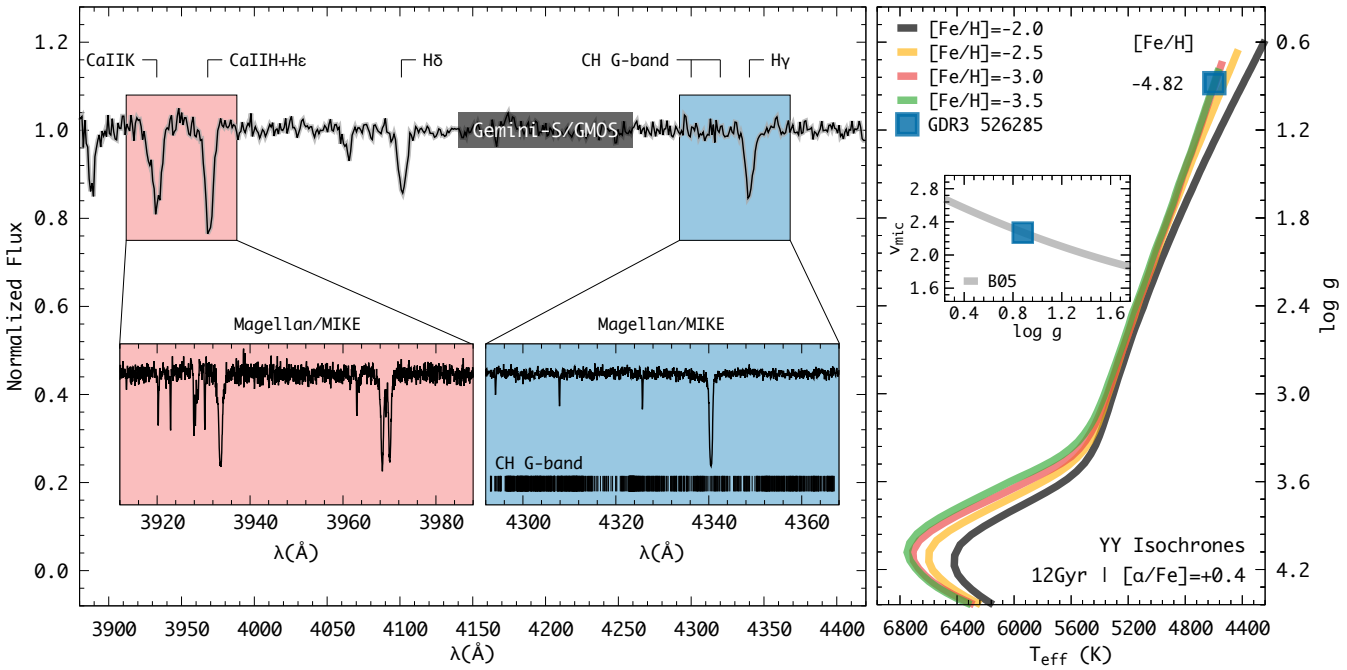

Figure 1. Left: normalized spectra of GDR3_526285. The medium-resolution GMOS spectrum ($\mathcal{R} \sim 1500$; see text) is shown in the upper portion of this panel. Red and blue insets highlight spectral features of interest in our high-resolution MIKE spectrum ($\mathcal{R} \sim 35k$; Section 2.2), namely Ca II K and H ($3920 \lesssim \lambda/\text{Å} \lesssim 3980$) and CH G band ($\sim$4300 Å), respectively. Right: 12 Gyr, α-enhanced Y^2 isochrones (S. Yi et al. 2001; P. Demarque et al. 2004) in $T_{\rm eff}$ vs. $\log g$ space at, from right to left, [Fe/H] $= -2$ (black), -2.5 (yellow), -3 (orange), and -3.5 (green). The inset panel shows the quadratic $\log g$–ξ relation from P. S. Barklem et al. (2005; fit by A. P. Ji et al. 2023, gray line). Star GDR3_526285 is plotted as the blue square.

Spectroscopy Made Harder (`smhr`; A. R. Casey et al. 2025) code.[15] We find a heliocentric-corrected $v_{\rm los} = +428.7$ km s^{-1}. Due to slit centering and λ calibration, MIKE spectra carry a $\sim$2 km s^{-1} systematic error floor at the resolution and S/N of our data (see A. P. Ji et al. 2020b; V. M. Placco et al. 2025).

3. Methods

3.1. Stellar Parameters

We obtain stellar parameters for GDR3_526285 using a combination of multiband photometric data and our MIKE spectrum. We apply color–$T_{\rm eff}$–[Fe/H] calibrations from A. Mucciarelli et al. (2021), assuming [Fe/H] $= -4$ and G, BP, RP Gaia DR3 photometry and K magnitude from the Two Micron All Sky Survey (2MASS; M. F. Skrutskie et al. 2006); Table 1 compiles relevant information. We compute 10^4 realizations of each of six possible color combinations accounting for the observed (Gaussian) uncertainties. Then, the final $T_{\rm eff}$ value is taken as the weighted average between the medians and median absolute deviations of the resulting distributions.

We point out that GDR3_526285 is located in a Galactic region of significant reddening at $E(B-V) = 0.1622$ (E. F. Schlafly & D. P. Finkbeiner 2011), which has a major impact on the inferred $T_{\rm eff}$. Hence, we consider the possibility of an overestimated reddening due to, e.g., the presence of the Magellanic gas stream (D. L. Nidever et al. 2010) given the on-sky position of GDR3_526285 (see Section 4 below). However, we notice that, even in the densest region of the Magellanic stream, within the bridge between the LMC and Small Magellanic Cloud (SMC), the E. F. Schlafly & D. P. Finkbeiner (2011) $E(B-V)$ is not as high. Therefore, we evaluate that the somewhat high reddening is very likely due to the location of GDR3_526285 near the Galactic plane (Galactic latitude $b = -24.2595$). Still, we note that previous studies of high-reddening metal-poor stars (e.g., P. Bonifacio et al. 2000) performed their own corrections to the $E(B-V)$ values from, e.g., the D. J. Schlegel et al. (1998) dust map. Using Equation (1) from P. Bonifacio et al. (2000) would here result in $E(B-V) = 0.158$, which is essentially the E. F. Schlafly & D. P. Finkbeiner (2011) value. Finally, considering a putative case of no extinction, the derived $T_{\rm eff}$ with our method would then be $\approx$4320 K. Such a cooler atmosphere would lead to an iron abundance of [Fe/H] < -5 for GDR3_526285. As a result, we adopt the E. F. Schlafly & D. P. Finkbeiner (2011) value, which is, in fact, a conservative choice with regards to the low metallicity of our star.

We compare GDR3_526285's $T_{\rm eff}$ value with the most metal-poor models available in the Yonsei–Yale (Y^2) set of isochrones (S. Yi et al. 2001; P. Demarque et al. 2004). We particularly adopt a 12 Gyr Y^2 track with [Fe/H] $= -3.5$ and α enhancement of [α/Fe] $= +0.4$. We interpolate this isochrone with $T_{\rm eff}$ uncertainties to find $\log g$ according to an RGB solution (right panel of Figure 1). We note that Gaia DR3 astrometric catalog has a negative parallax value for GDR3_526285 despite it being relatively bright at $G \approx 15$, reinforcing that this object is a distant giant rather than a nearby main-sequence star. We then calculate GDR3_526285's microturbulence velocity (ξ) from the empirical $\log g$–ξ quadratic relation from A. P. Ji et al. (2023) based on P. S. Barklem et al. (2005) data. We underscore that a different $\log g$–ξ relation, e.g., with I. U. Roederer et al. (2014) parameters for RGB stars, yields ξ values up to $\sim$0.5 km s^{-1} lower. Fixing all other stellar parameters, this would bring the [Fe/H] of GDR3_526285 to a value 0.13 dex higher. Since this is within our formal 1σ iron-

[15] https://github.com/andycasey/smhr

Table 1
Observational Data for Gaia DR3 5262850721755411072

Quantity	Symbol	Value	Unit	Source	Reference
R.A.	α (J2000)	108.91087	deg	Gaia DR3	Gaia Collaboration et al. (2023)
Decl.	δ (J2000)	−73.58142	deg	Gaia DR3	Gaia Collaboration et al. (2023)
Galactic Longitude	ℓ	284.97496	deg	Gaia DR3	Gaia Collaboration et al. (2023)
Galactic Latitude	b	−24.25953	deg	Gaia DR3	Gaia Collaboration et al. (2023)
Parallax	ϖ	-0.0064 ± 0.0172	mas	Gaia DR3	Gaia Collaboration et al. (2023)
Proper Motion (α)	$\mu_{\alpha,*}$[a]	3.767 ± 0.022	mas yr^{-1}	Gaia DR3	Gaia Collaboration et al. (2023)
Proper Motion (δ)	μ_δ	2.627 ± 0.022	mas yr^{-1}	Gaia DR3	Gaia Collaboration et al. (2023)
Mass	$M_\star$	0.78 ± 0.10	$M_\odot$	Assumed	This work
B Magnitude	*B*	16.467	mag	APASS[b] DR9	A. A. Henden et al. (2016)
V Magnitude	*V*	15.362	mag	APASS DR9	A. A. Henden et al. (2016)
G Magnitude	*G*	14.995	mag	Gaia DR3	Gaia Collaboration et al. (2023)
BP Magnitude	*BP*	15.648	mag	Gaia DR3	Gaia Collaboration et al. (2023)
RP Magnitude	*RP*	14.203	mag	Gaia DR3	Gaia Collaboration et al. (2023)
J Magnitude	*J*	13.161	mag	2MASS	⋯
H Magnitude	*H*	12.579	mag	2MASS	M. F. Skrutskie et al. (2006)
K Magnitude	*K*	12.466	mag	2MASS	M. F. Skrutskie et al. (2006)
*W*1 Magnitude	*W*1	12.311	mag	AllWISE[c]	R. M. Cutri et al. (2021)
*W*2 Magnitude	*W*2	12.272	mag	AllWISE	R. M. Cutri et al. (2021)
g Magnitude	*g*	15.682	mag	SkyMapper DR4	C. A. Onken et al. (2024)
r Magnitude	*r*	15.053	mag	SkyMapper DR4	C. A. Onken et al. (2024)
i Magnitude	*i*	14.550	mag	SkyMapper DR4	C. A. Onken et al. (2024)
z Magnitude	*z*	14.304	mag	SkyMapper DR4	C. A. Onken et al. (2024)
Color Excess	$E(B-V)$	0.1622	mag	IRSA[d]	E. F. Schlafly & D. P. Finkbeiner (2011)
Extinction (V)	A_V	0.503	mag	Equation (2)	E. F. Schlafly & D. P. Finkbeiner (2011)
Extinction (G)	A_G	0.397 ± 0.005	mag	Equation (3)	S. Wang & X. Chen (2019)
Bolometric Correction	BC(G)	-0.568 ± 0.022	mag	`bcutil`[e]	L. Casagrande & D. A. VandenBerg (2018)
Line-of-sight Velocity	$v_{\rm los}$	$+428.7 \pm 2.0$	km s^{-1}	MIKE/Magellan	This work
Effective Temperature	$T_{\rm eff}$	4596 ± 65	K	color–$T_{\rm eff}$–[Fe/H][f]	This work
		4742	K	Data driven	R. Andrae et al. (2023)
		4803^{+161}_{-51}	K	`StarHorse`	F. Anders et al. (2022)
Log of Surface Gravity	$\log g$	0.88 ± 0.15	[cgs]	Isochrone[g]	This work
		1.38	[cgs]	Data driven	R. Andrae et al. (2023)
		$1.52^{+0.18}_{-0.25}$	[cgs]	`StarHorse`	F. Anders et al. (2022)
Microturbulence Velocity	ξ	2.27 ± 0.10	km s^{-1}	$\log g$–ξ[h]	This work
Metallicity	[Fe/H]	-4.82 ± 0.25	dex	MIKE/Magellan	This work
		−3.5	dex	Data driven	This work
		−2.9	dex	Data driven	R. Andrae et al. (2023)
		<-2.9	dex	Model grid	M. K. Mardini et al. (2025, in preparation)
Distance Modulus	μ	16.9 ± 0.4	mag	Equation (1)	This work
Heliocentric Distance	$d_{\rm helio}$	$24.1^{+4.9}_{-4.1}$	kpc	$10^{[(\mu+5)/5]-3}$	This work
		$15.8^{+3.4}_{-4.2}$	kpc	`StarHorse`	F. Anders et al. (2022)

Notes.
[a] $\mu_{\alpha,*} = \mu_\alpha \cos\delta$.
[b] The AAVSO Photometric All-Sky Survey.
[c] Wide-field Infrared Survey Explorer.
[d] Infrared Science Archive (https://irsa.ipac.caltech.edu/).
[e] https://github.com/casaluca/bolometric-corrections/tree/master
[f] A. Mucciarelli et al. (2021).
[g] S. Yi et al. (2001); P. Demarque et al. (2004).
[h] P. S. Barklem et al. (2005; quadratic fit by A. P. Ji et al. 2023).

abundance uncertainty (Table 2), we consider our estimate of ξ to be appropriate.

With $T_{\rm eff}$, $\log g$, and ξ fixed, we derive the iron abundance/metallicity for GDR3_526285 from the equivalent widths (Gaussian fits) of 30 Fe I lines in the `smhr` environment. We use an F. Castelli & R. L. Kurucz (2003) 1D plane-parallel model atmosphere with no overshooting and [M/H] = −4.0. `smhr` runs the 2017 version of radiative transfer code `MOOG` (C. A. Sneden 1973), with scattering (J. S. Sobeck et al. 2011),[16] under the assumption of local thermodynamic equilibrium (LTE). The final [Fe/H], and other atmospheric parameters ($T_{\rm eff}$, $\log g$, ξ), are shown in Table 1.

[16] https://github.com/alexji/moog17scat

Table 2
Abundances for Individual Species

Species	$\log \epsilon_{\odot}$ (X)	$\log \epsilon$ (X)	[X/H]	[X/Fe]	σ	N
C	8.43	<4.11	<−4.32	<+0.50	⋯	⋯
C_{cor}[a]	8.43	<4.79	<−3.64	<+1.18	⋯	⋯
Na I	6.24	1.77	−4.47	+0.35	0.10	2
Mg I	7.60	2.94	−4.66	+0.16	0.10	5
Al I	6.45	1.24	−5.21	−0.39	0.10	2
Si I	7.51	2.85	−4.66	+0.16	0.15	1
Ca I	6.34	1.36	−4.98	−0.16	0.15	1
Sc II	3.15	−1.65	−4.79	+0.03	0.15	1
Ti II	4.95	0.21	−4.74	+0.09	0.10	4
Cr I	5.64	0.29	−5.35	−0.53	0.15	1
Fe I	7.50	2.68	−4.82	0.00	0.25	30
Ni I	6.22	1.62	−4.60	+0.22	0.15	1

Note.
[a] Applying the evolutionary carbon correction (Δ[C/Fe] = +0.68) from V. M. Placco et al. (2014).

For our kinematic analysis, we require an estimate of GDR3_526285's heliocentric distance ($d_{\rm helio}$). We employ the fundamental relation

$$\log g = 4.44 + \log M_{\star} + 4\log\left(\frac{T_{\rm eff}}{5780\ {\rm K}}\right) + 0.4(G_0 - \quad + {\rm BC}(G) - M_{\rm bol,\odot}) \quad (1)$$

to derive a distance modulus (μ), where $M_{\star} = 0.78 \pm 0.1\,M_{\odot}$ is the assumed mass of GDR3_526285 (following F. O. Barbosa et al. 2025), G_0 is the extinction-corrected Gaia G magnitude, BC(G) is the corresponding bolometric correction (L. Casagrande & D. A. VandenBerg 2018), and $M_{\rm bol,\odot} = 4.75$ is the bolometric magnitude of the Sun (see K. A. Venn et al. 2017; I. U. Roederer et al. 2018; A. P. Ji et al. 2020a). To obtain G_0, we utilize the extinction law from S. Wang & X. Chen (2019) with $R_V = 3.1$:

$$A_V = R_V \cdot E(B - V), \quad (2)$$

$$A_G = (0.789 \pm 0.005) \cdot A_V, \quad (3)$$

$$G_0 = G - A_G, \quad (4)$$

where A_V and A_G are the extinction values in V and G bands, respectively, and $E(B - V)$ is the E. F. Schlafly & D. P. Finkbeiner (2011) color excess. We list the resulting μ and $d_{\rm helio}$, as well as other quantities used, in Table 1.

3.2. Chemical Abundances and Upper Limits

Abundances for chemical species beyond Fe I are also determined with the MOOG 2017 version within smhr. The molecular and atomic line list is taken from the linemake[17] compilation (V. M. Placco et al. 2021b). We default to equivalent widths (Gaussian fits) to measure abundances for Na I, Mg I, Ca I, Sc II, Ti II, Cr I, and Ni I. For the CH band as well as for blended features, i.e., Al I and Si I, we use the spectral synthesis technique. The number of lines detected for each element/ion (N) and final abundances and abundance ratios are in Table 2, assuming the M. Asplund et al. (2009) solar atmospheric composition. For species where $N = 1$, we assume an uncertainty floor of 0.15 dex.

Figure 2 shows the determination of the upper limit on carbon, using the method outlined in V. M. Placco et al. (2024). Briefly, we define the A(C) upper limit as the abundance for which the χ^2 matches the value for a spectrum without any carbon on the opposite side of the global minimum. The top panel shows the GDR3_526285 spectrum (blue squares and line, smoothed using a moving average of size 3), compared to a synthetic spectrum with no carbon (black line). The magenta line represents the carbon upper limit of A(C) = 4.11, [C/Fe] = +0.50. The bottom panels show the χ^2 minimization technique, applied to four 2.5 Å sections within the carbon G band. The adopted upper limit is the highest out of the four individual values.

3.3. Kinematics

We compute Cartesian Galactocentric positions $\boldsymbol{r} = (X, Y, Z)$ and velocities $\boldsymbol{v} = (V_X, V_Y, V_Z)$ for GDR3_526285 from phase-space information in Table 1 using Astropy tools (v5.3.4; Astropy Collaboration et al. 2013, 2018). We adopt the distance and velocity of the Sun with respect to the Galactic center to be $\sqrt{X_{\odot}^2 + Y_{\odot}^2} = R_{\odot} = 8.122$ kpc, with no vertical displacement from the Milky Way's plane, and $(V_R, V_{\phi}, V_Z)_{\odot} = (-12.9, 245.6, 7.8)$ km s^{-1} in cylindrical frame,[18] respectively (R. Drimmel & E. Poggio 2018; Gravity Collaboration et al. 2018). With $\boldsymbol{r}$ and $\boldsymbol{v}$, we calculate the total orbital energy $E_{\rm tot} = \frac{1}{2}(V_X^2 + V_Y^2 + V_Z^2) + \Phi(\boldsymbol{r})$ for GDR3_526285 in the axisymmetric Galactic model potential Φ of P. J. McMillan (2017). We also use the angular-momentum vector $\boldsymbol{L} = (L_X, L_Y, L_Z)$[19] for our interpretations. Note that $E_{\rm tot} < 0$ signifies that a given object is formally bound to the model potential Φ and $RV_{\phi} = L_Z < 0$ denotes prograde motion .

4. Results

Our analysis based on multiband photometry and high-resolution spectroscopy confirms that GDR3_526285 is a distant ($d_{\rm helio} = 24.1^{+4.9}_{-4.1}$) RGB star (4596 ± 65 K, $\log g = 0.88 \pm 0.15$) in the Milky Way's halo. Comparing SkyMapper's DR4 (C. A. Onken et al. 2024) $g - r$ color (Table 1) to a MESA Isochrones and Stellar Tracks (A. Dotter 2016; J. Choi et al. 2016) 12.5 Gyr, [Fe/H] = −3 solar-scaled isochrone, we find similar $\mu \approx 17.2$ or $d_{\rm helio} \approx 27.5$ kpc.

We note that the astrophotometric $d_{\rm helio}$ value for GDR3_526285 derived by F. Anders et al. (2022, $15.8^{+3.4}_{-4.2}$ kpc) with the StarHorse code (B. X. Santiago et al. 2016; A. B. A. Queiroz et al. 2018) is significantly lower than our own estimate. This $d_{\rm helio}$ discrepancy might be due to a limitation of StarHorse's adopted stellar model grid that only reaches [M/H] = −2.2 at its metal-poor end; at a given $T_{\rm eff}$, lower-metallicity isochrones require $\log g$ to be lower (see various isochrones in Figure 1), which translates into a meaningful difference in the predicted μ (Equation (1)), and hence $d_{\rm helio}$. Moreover, Gaia's negative parallax measurement is uninformative and StarHorse's $d_{\rm helio}$ estimate could be dominated by the assumed underlying Milky Way geometric prior, whereas, toward the on-sky location of GDR3_526285, the outer Galactic halo is likely

[17] https://github.com/vmplacco/linemake

[18] $V_R = (XV_X + YV_Y)/R$ and $V_{\phi} = (XV_Y - YV_X)/R$.

[19] $L_X = YV_Z - ZV_Y$, $L_Y = ZV_X - XV_Z$, $L_Z = XV_Y - YV_X$.

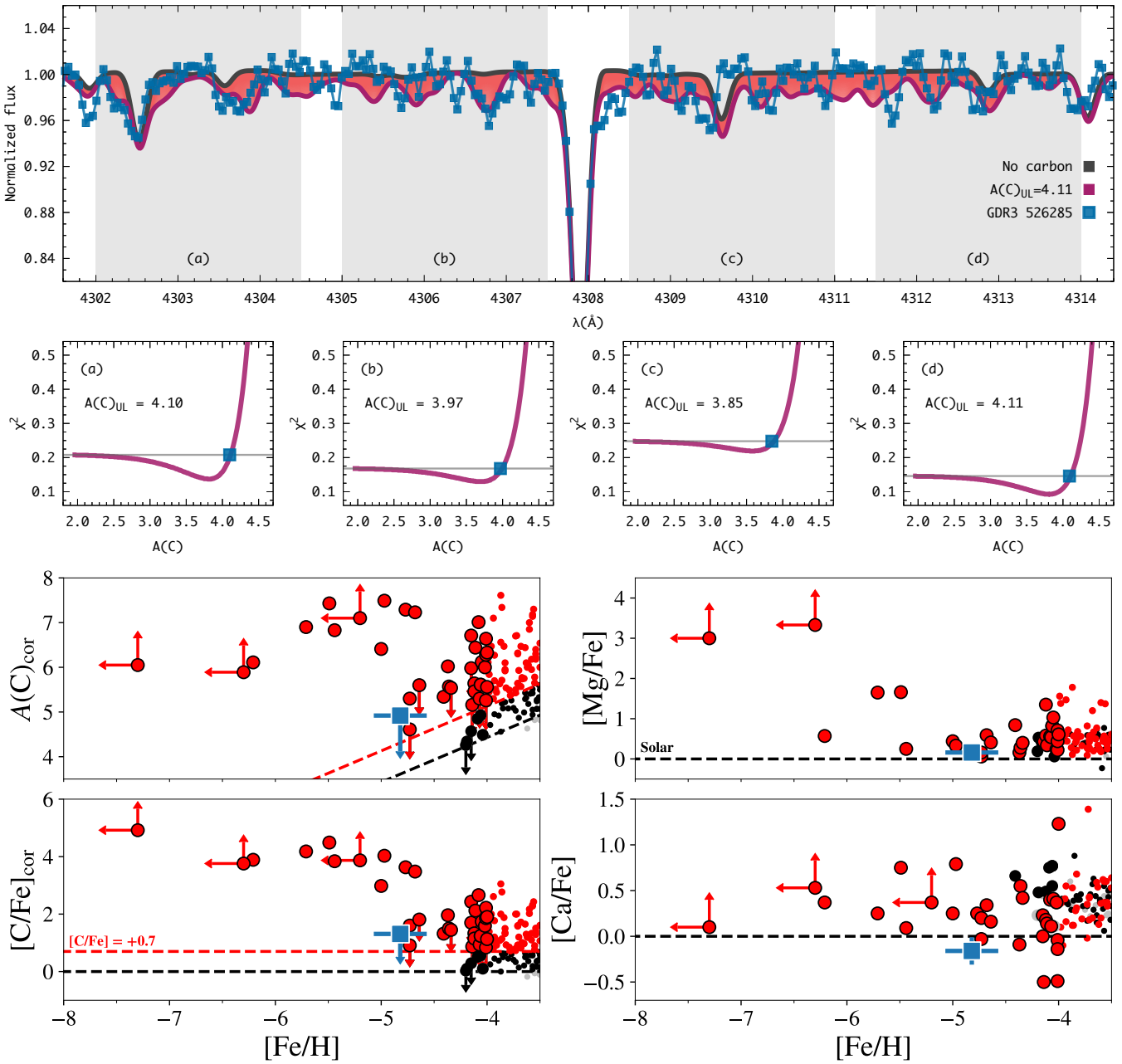

Figure 2. Top panel: MIKE spectrum of GDR3_526285 around the CH *G* band (blue squares); $4300 \leqslant \lambda/\text{Å} \leqslant 4316$. Our final $A(\text{C}) = 4.11$ upper limit is represented by the solid magenta line. The difference between our A(C) upper limit and the no-carbon case is shown as the red region within magenta and black lines. Panels (a), (b), (c), and (d) illustrate different λ windows used in our χ^2 minimization method to derive the carbon-abundance upper limit (Section 3.2). Bottom panels: key elemental abundance ratios that characterize UMP stars: $A(\text{C})_{\text{cor}}$, $[\text{C/Fe}]_{\text{cor}}$, [Mg/Fe], and [Ca/Fe] as a function of [Fe/H], where the subscript "cor" indicates carbon abundances with applied evolutionary corrections (V. M. Placco et al. 2014). Small dots are non-UMP stars ([Fe/H] > -4) compiled from the SAGA database and JINAbase (T. Suda et al. 2008; A. Abohalima & A. Frebel 2018), while the UMP stars are shown with larger circles. Symbols are colored according to stellar [C/Fe] ratios: subsolar in gray, $0 \leqslant [\text{C/Fe}] < +0.7$ in black, and CEMP stars in red. Upper/lower limits are plotted with arrows. In the carbon-abundance panels on the left, the red dashed lines mark this [C/Fe] $= +0.7$ boundary for CEMP classification. Black dashed lines denote solar levels in all panels. GDR3_526285 is the blue square (Table 2).

significantly perturbed by the presence of the LMC. To confirm this hypothesis, we calculate another d_{helio} value with an exponentially decreasing space density prior following the method by M. K. Mardini et al. (2022). We find a d_{helio} of 16.0 ± 2.8 kpc, which is 1σ compatible with the `StarHorse` value. We conclude that the d_{helio} reported by F. Anders et al. (2022) is biased low due to either one of these described effects or a combination thereof.

Beyond the extraordinarily low iron abundance of GDR3_526285, perhaps the most remarkable feature of this UMP star is the relatively low upper limit on the [C/Fe] compared with other stars at a similar [Fe/H]. There are two other known UMP stars at [Fe/H] < -4.5 with potentially similarly low carbon abundances, SDSS J102915+172927 (E. Caffau et al. 2011) and Pristine_221.8781+9.7844 (E. Starkenburg et al. 2018). The latter has a relatively meaningless, high carbon-abundance upper limit ([C/Fe] $< +1.81$) compared to the former ([C/Fe] $< +0.91$), when assuming the M. Asplund et al. (2009) solar chemical composition and LTE.

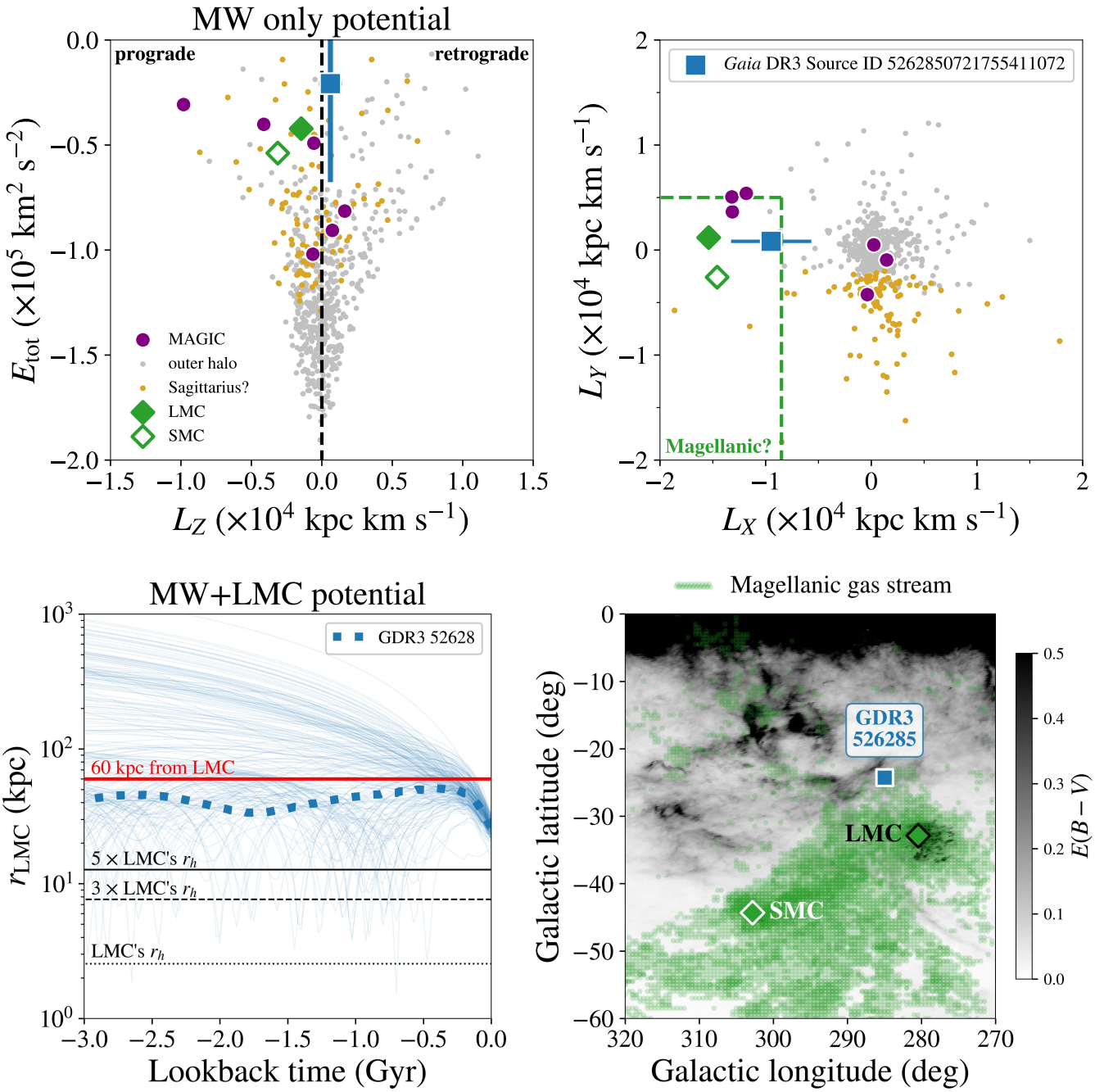

Figure 3. Upper left: (L_Z, $E_{\rm tot}$); see text for discussion. Upper right: (L_X, L_Y). Gray and yellow dots are distant ($\geqslant$35 kpc) low-metallicity ([Fe/H] < -2.5) halo stars (G. Limberg et al. 2023), where the latter are presumably associated with the Sagittarius stellar stream (B. D. Johnson et al. 2020). Purple circles are outer-halo extremely metal-poor stars ([Fe/H] < -3) from the MAGIC survey (V. M. Placco et al. 2025). Green diamonds are the LMC (filled) and SMC (empty) based on phase-space information compiled by A. B. Pace (2024; github.com/apace7/local_volume_database). Green dashed lines in (L_X, L_Y) space delineate plausible association with the proposed Magellanic stellar stream (V. Chandra et al. 2023). In both upper panels, GDR3_526285 is represented by the blue square. Bottom left: 200 realizations of GDR3_526285's orbit (thin blue lines, with mean trajectory as the dotted one) in a time-varying model potential that includes both the Milky Way and the infalling LMC (E. Vasiliev et al. 2021). This panel depicts GDR3_526285's distance to the LMC ($r_{\rm LMC}$) as a function of lookback time (backward orbit). Bottom right: on-sky location of GDR3_526285, SMC, and LMC in Galactic coordinates. The distribution of $E(B-V)$ values from the D. J. Schlegel et al. (1998) dust map is displayed as the grayscale background, with darker regions depicting higher reddening. The Magellanic gas stream (D. L. Nidever et al. 2010) is overlaid in transparent green.

The observed A(C) < 4.11 upper limit we derive for GDR3_526285 is, in fact, nominally lower than the one for SDSS J102915+172927 with A(C) < 4.61 (E. Caffau et al. 2024). However, GDR3_526285 is an evolved RGB star, and, if we compensate for the expected carbon depletion due to CN processing during stellar evolution (Δ[C/Fe] $= +0.68$; V. M. Placco et al. 2014), the final value we adopt is A(C) < 4.79, leading to [C/Fe] $< +1.18$ (bottom panels in Figure 2). Future spectroscopic observations with higher S/N at $\sim$4300 Å will be needed to provide a more stringent constraint on the carbon abundance of GDR3_526285. Moreover, departures from the 1D atmosphere and LTE assumptions affect cool metal-poor stars more profoundly, which would be the case for GDR3_526285 (e.g., M. Asplund 2005).

Specifically for UMP ([Fe/H] = −4) RGB stars, S. A. Popa et al. (2023) estimated corrections of about +0.2 dex in [C/Fe] from the CH *G* band. Hence, future 3D non-LTE analysis of this star is also highly desirable.

The potential non-CEMP nature of GDR3_526285 along with its low iron abundance suggests that this stars has one of the lowest overall metal (atomic number > 2) mass fractions known, likely similar to that of SDSS J102915+172927. Consequently, GDR3_526285 could provide important constraints on the physics of early star formation in exceptionally metal-poor environments at redshift $z > 10$. For example, according to the critical threshold established by A. Frebel et al. (2007) for the cooling levels required for facilitating early low-mass star formation ($D_{\rm trans} \equiv \log_{10}[10^{[C/H]} + 0.3 \times 10^{[O/H]}]$), given our upper limit of $[C/H]_{\rm cor} < -3.64$ and adopting oxygen enhancement of [O/Fe] = +0.6, leads to $D_{\rm trans} < -3.6$. Even assuming [O/Fe] = +1.6 only changes it to $D_{\rm trans} \lesssim -3.4$. These limits are close to the critical threshold of $D_{\rm trans,crit} \sim -3.5 \pm 0.2$, and future observations may well show this star to be below the critical value. As such, GDR3_526285 likely formed from dust-cooled gas (G. Chiaki et al. 2017 and references therein) rather than fine-structure line cooling due to carbon and/or oxygen present in primordial gas.

We estimate the overall metal mass fraction Z for GDR3_526285 considering *only* the elements/abundances from Table 2. As in E. Caffau et al. (2011), we assume both oxygen- and nitrogen-to-iron ratios to be [O or N/Fe] = +0.6. For this calculation, we adopt the number ratio between helium and hydrogen atoms to be 1/12. We find $Z_{\rm GDR3-526585} \lesssim 1.0 \times 10^{-6}$ for GDR3_526285. Using the same species and LTE values reported in E. Caffau et al. (2024) for SDSS J102915+172927 leads to $Z_{\rm Caffau+24} \lesssim 9.2 \times 10^{-7}$. At least these two stars support a star formation mechanism in near-metal-free, dust-cooled environments.

Regarding the kinematics/dynamics, GDR3_526285 has a high orbital energy $E_{\rm tot} \gtrsim -0.5 \times 10^5$ km^2 s^{-2} (P. J. McMillan 2017 model potential) and an immense X-component of angular momentum $L_X = -9476^{+3458}_{-4140}$ kpc km s^{-1}. These are commensurate with its large $d_{\rm helio}$, proper motions, and $v_{\rm los}$ (Table 1). Similarly to high-$E_{\rm tot}$ extremely metal-poor ([Fe/H] < −3) outer-halo stars recently discovered in the MAGIC survey (V. M. Placco et al. 2025; purple symbols in Figure 3), it is plausible that the orbit of GDR3_526285 was perturbed by the infall of the LMC (e.g., E. Vasiliev 2023). Another possibility is that GDR3_526285 was originally part of the Magellanic system but has since been stripped by the Milky Way. If this latter hypothesis can be confirmed, GDR3_526285 might be linked to another UMP (non-CEMP) star in the LMC (A. Chiti et al. 2024). The top right panel in Figure 3 shows, in (L_X, L_Y) space, the cuts from V. Chandra et al. (2023) to isolate Magellanic stellar debris, and GDR3_526285 is located just within this region. The on-sky position of GDR3_526285 in comparison to both SMC and LMC is presented in the bottom right panel of the same figure.

Given the hint from angular-momentum space that GDR3_526285 might have a Magellanic origin, we implement a Monte Carlo experiment similar to that of V. Chandra et al. (2023) to further evaluate this possibility. We integrate orbits for 3 Gyr backward in a time-varying potential that includes both the Milky Way and the infalling LMC (E. Vasiliev et al. 2021). In this model potential, the Milky Way stellar distribution is similar to that in P. J. McMillan (2017), but with a triaxial dark-matter halo. The total assumed mass of the LMC is $M_{\rm LMC} = 1.5 \times 10^{11} M_\odot$. We sample 1000 orbits for GDR3_526285 from the uncertainties in the observed phase-space quantities. The results of this exercise are shown in the bottom left panel of Figure 3. A realization is considered to have become bound to the LMC whenever it experiences a pericenter of <60 kpc with respect to the LMC's center at ⩾2 Gyr ago (V. Chandra et al. 2023 criterion; see the red solid line). The fraction of realizations where GDR3_526285 becomes bound to the LMC is 53.1%, which reinforces a Magellanic association.

5. Summary

We have reported the discovery of a UMP star ([Fe/H] = −4.82 ± 0.25) which has one of the lowest iron abundances ever measured. For reference, a search in both SAGA (T. Suda et al. 2008) and the most up-to-date version of JINAbase[20] (A. Abohalima & A. Frebel 2018) reveals only ∼15 stars known at [Fe/H] ≲ −4.5 (e.g., N. Christlieb et al. 2004; A. Frebel et al. 2005, 2015; T. Hansen et al. 2014; P. Bonifacio et al. 2015, 2018; E. Caffau et al. 2016; E. Starkenburg et al. 2018; A. Frebel et al. 2019; T. Nordlander et al. 2019), including the aforementioned SMSS J031300.36−670839.3 (S. C. Keller et al. 2014) and SDSS J102915+172927 (E. Caffau et al. 2011, 2024). We note, however, that this exact number is susceptible to variations given uncertainties in [Fe/H] as well as 3D and non-LTE effects (J. E. Norris & D. Yong 2019).

We have identified this extraordinary star among the Gaia DR3 low-resolution XP spectra and combined multiband photometry with high-resolution spectroscopy to derive stellar parameters and chemical abundances. Our analysis confirmed that GDR3_526285 is a distant ($d_{\rm helio} \approx 24$ kpc) RGB star ($T_{\rm eff} = 4596$ K, $\log g = 0.88$) in the Milky Way's halo. The star has an upper limit of $[C/Fe]_{\rm cor} < +1.18$ (after applying the V. M. Placco et al. 2014 evolutionary correction), which suggests that it does not have a strong carbon overabundance as other stars with [Fe/H] < −4.5. This discovery highlights the potential of an all-sky search for low-metallicity targets with Gaia XP and demonstrates that this strategy is a powerful "treasure map" for finding UMP stars.

Given the incredibly low abundances of [Fe/H] combined with no strong carbon enhancement, GDR3_526285 has an overall metal mass fraction of $Z_{\rm GDR3-526585} \lesssim 1.0 \times 10^{-6}$, which is comparable to that of SDSS J102915+172927 (E. Caffau et al. 2011, 2024). Future higher-S/N spectroscopic observations combined with 3D non-LTE modeling are of high interest to achieve a tighter upper limit on the carbon abundance and perhaps a measurement of nitrogen, which has a major impact on the estimated overall metallicity. Finally, the kinematics of GDR3_526285 make it tentatively linked to the Magellanic system, either by being dynamically perturbed by its recent infall or as a former LMC star that has been tidally stripped by the Milky Way. We have performed a Monte Carlo experiment in a Milky Way+LMC potential and found that, for 53.1% of the sampled orbits, GDR3_526285 indeed ended up bound to the LMC, pointing to a Magellanic origin.

Acknowledgments

We thank the referee for useful comments and suggestions that contributed to this Letter. G.L. is indebted to all those

[20] https://github.com/Mohammad-Mardini/JINAbase-updated/

involved with the multi-institutional Milky Way BR Group for the weekly discussions. G.L. is particularly thankful to Hélio Perottoni, who provided feedback on an early version of this Letter, and Fred Anders, for assistance with `StarHorse` outputs and priors. G.L. acknowledges support from KICP/UChicago through a KICP Postdoctoral Fellowship. The work of V.M.P. is supported by NOIRLab, which is managed by the Association of Universities for Research in Astronomy (AURA) under a cooperative agreement with the U.S. National Science Foundation. A.C. is supported by a Brinson Prize Fellowship at KICP/UChicago. S.R. acknowledges partial financial support from FAPESP (proc. 2020/15245-2), CNPq (proc. 303816/2022-8), and CAPES. A.F. acknowledge support from NSF-AAG grant AST-2307436. This research is partially based on observations obtained under program GS-2023B-Q-107 at the international Gemini Observatory.

This work has made use of data from the European Space Agency (ESA) mission Gaia (https://www.cosmos.esa.int/gaia), processed by the Gaia Data Processing and Analysis Consortium (DPAC, https://www.cosmos.esa.int/web/gaia/dpac/consortium). Funding for the DPAC has been provided by national institutions, in particular the institutions participating in the Gaia Multilateral Agreement.

ORCID iDs

Guilherme Limberg https://orcid.org/0000-0002-9269-8287
Vinicius M. Placco https://orcid.org/0000-0003-4479-1265
Alexander P. Ji https://orcid.org/0000-0002-4863-8842
Anirudh Chiti https://orcid.org/0000-0002-7155-679X
Mohammad K. Mardini https://orcid.org/0000-0001-9178-3992
Anna Frebel https://orcid.org/0000-0002-2139-7145
Silvia Rossi https://orcid.org/0000-0001-7479-5756

References

Abohalima, A., & Frebel, A. 2018, ApJS, 238, 36
Aguado, D. S., Youakim, K., González Hernández, J. I., et al. 2019, MNRAS, 490, 2241
Anders, F., Khalatyan, A., Queiroz, A. B. A., et al. 2022, A&A, 658, A91
Andrae, R., Rix, H.-W., & Chandra, V. 2023, ApJS, 267, 8
Aoki, W., Beers, T. C., Christlieb, N., et al. 2007, ApJ, 655, 492
Arentsen, A., Placco, V. M., Lee, Y. S., et al. 2022, MNRAS, 515, 4082
Asplund, M. 2005, ARA&A, 43, 481
Asplund, M., Grevesse, N., Sauval, A. J., & Scott, P. 2009, ARA&A, 47, 481
Astropy Collaboration, Price-Whelan, A. M., Sipőcz, B. M., et al. 2018, AJ, 156, 123
Astropy Collaboration, Robitaille, T. P., Tollerud, E. J., et al. 2013, A&A, 558, A33
Barbosa, F. O., Chiti, A., Limberg, G., et al. 2025, arXiv:2504.03593
Barklem, P. S., Christlieb, N., Beers, T. C., et al. 2005, A&A, 439, 129
Beers, T. C., & Christlieb, N. 2005, ARA&A, 43, 531
Bernstein, R., Shectman, S. A., Gunnels, S. M., Mochnacki, S., & Athey, A. E. 2003, Proc. SPIE, 4841, 1694
Bonifacio, P., Caffau, E., François, P., & Spite, M. 2025, A&ARv, 33, 2
Bonifacio, P., Caffau, E., Spite, M., et al. 2015, A&A, 579, A28
Bonifacio, P., Caffau, E., Spite, M., et al. 2018, A&A, 612, A65
Bonifacio, P., Monai, S., & Beers, T. C. 2000, AJ, 120, 2065
Caffau, E., Bonifacio, P., François, P., et al. 2011, Natur, 477, 67
Caffau, E., Bonifacio, P., Monaco, L., et al. 2024, A&A, 691, A245
Caffau, E., Bonifacio, P., Spite, M., et al. 2016, A&A, 595, L6
Casagrande, L., & VandenBerg, D. A. 2018, MNRAS, 479, L102
Casey, A. R., Ji, A., & Holmbeck, E. 2025, smhr: Automatic Curve-of-growth Analyses of High-resolution Stellar Spectra, Astrophysics Source Code Library, ascl:2502.025
Castelli, F., & Kurucz, R. L. 2003, in Modeling of Stellar Atmospheres IAU Symp. 210, Modelling of Stellar Atmospheres, Poster Contributions, ed. N. Piskunov, W. W. Weiss, & D. F. Gray (Cambridge: Cambridge Univ. Press), A20
Cayrel, R., Depagne, E., Spite, M., et al. 2004, A&A, 416, 1117
Cenarro, A. J., Moles, M., Cristóbal-Hornillos, D., et al. 2019, A&A, 622, A176
Chandra, V., Naidu, R. P., Conroy, C., et al. 2023, ApJ, 956, 110
Chen, T., & Guestrin, C. 2016, arXiv:1603.02754
Chiaki, G., Tominaga, N., & Nozawa, T. 2017, MNRAS, 472, L115
Chiti, A., Mardini, M., Limberg, G., et al. 2024, NatAs, 8, 637
Choi, J., Dotter, A., Conroy, C., et al. 2016, ApJ, 823, 102
Christlieb, N., Gustafsson, B., Korn, A. J., et al. 2004, ApJ, 603, 708
Cohen, J. G., Christlieb, N., Thompson, I., et al. 2013, ApJ, 778, 56
Curti, M., Maiolino, R., Curtis-Lake, E., et al. 2024, A&A, 684, A75
Cutri, R. M., Wright, E. L., Conrow, T., et al. 2021, yCat, 2328, 0
Davies, R. L., Allington-Smith, J. R., Bettess, P., et al. 1997, Proc. SPIE, 2871, 1099
De Angeli, F., Weiler, M., Montegriffo, P., et al. 2023, A&A, 674, A2
Demarque, P., Woo, J.-H., Kim, Y.-C., & Yi, S. K. 2004, ApJS, 155, 667
Dotter, A. 2016, ApJS, 222, 8
Drimmel, R., & Poggio, E. 2018, RNAAS, 2, 210
Frebel, A., Aoki, W., Christlieb, N., et al. 2005, Natur, 434, 871
Frebel, A., Chiti, A., Ji, A. P., Jacobson, H. R., & Placco, V. M. 2015, ApJL, 810, L27
Frebel, A., Ji, A. P., Ezzeddine, R., et al. 2019, ApJ, 871, 146
Frebel, A., Johnson, J. L., & Bromm, V. 2007, MNRAS, 380, L40
Frebel, A., & Norris, J. E. 2015, ARA&A, 53, 631
Gaia Collaboration, Prusti, T., de Bruijne, J. H. J., et al. 2016, A&A, 595, A1
Gaia Collaboration, Vallenari, A., Brown, A. G. A., et al. 2023, A&A, 674, A1
Galarza, C. A., Daflon, S., Placco, V. M., et al. 2022, A&A, 657, A35
Gimeno, G., Roth, K., Chiboucas, K., et al. 2016, Proc. SPIE, 9908, 99082S
Gravity Collaboration, Abuter, R., Amorim, A., et al. 2018, A&A, 615, L15
Hansen, T., Hansen, C. J., Christlieb, N., et al. 2014, ApJ, 787, 162
Heger, A., & Woosley, S. E. 2010, ApJ, 724, 341
Henden, A. A., Templeton, M., Terrell, D., et al. 2016, yCat, 2336, 0
Holmbeck, E. M., Hansen, T. T., Beers, T. C., et al. 2020, ApJS, 249, 30
Ishigaki, M. N., Tominaga, N., Kobayashi, C., & Nomoto, K. 2018, ApJ, 857, 46
Jacobson, H. R., Keller, S., Frebel, A., et al. 2015, ApJ, 807, 171
Ji, A. P., Li, T. S., Hansen, T. T., et al. 2020a, AJ, 160, 181
Ji, A. P., Li, T. S., Simon, J. D., et al. 2020b, ApJ, 889, 27
Ji, A. P., Simon, J. D., Roederer, I. U., et al. 2023, AJ, 165, 100
Johnson, B. D., Conroy, C., Naidu, R. P., et al. 2020, ApJ, 900, 103
Karovicova, I., White, T. R., Nordlander, T., et al. 2020, A&A, 640, A25
Keller, S. C., Bessell, M. S., Frebel, A., et al. 2014, Natur, 506, 463
Kelson, D. D. 2003, PASP, 115, 688
Labrie, K., Simpson, C., Cardenes, R., et al. 2023, RNAAS, 7, 214
Li, H., Aoki, W., Matsuno, T., et al. 2022, ApJ, 931, 147
Limberg, G., Queiroz, A. B. A., Perottoni, H. D., et al. 2023, ApJ, 946, 66
Mardini, M. K., Frebel, A., & Chiti, A. 2024, MNRAS, 529, L60
Mardini, M. K., Frebel, A., Chiti, A., et al. 2022, ApJ, 936, 78
McMillan, P. J. 2017, MNRAS, 465, 76
Mendes de Oliveira, C., Ribeiro, T., Schoenell, W., et al. 2019, MNRAS, 489, 241
Mucciarelli, A., Bellazzini, M., & Massari, D. 2021, A&A, 653, A90
Nidever, D. L., Majewski, S. R., Butler Burton, W., & Nigra, L. 2010, ApJ, 723, 1618
Nordlander, T., Bessell, M. S., Da Costa, G. S., et al. 2019, MNRAS, 488, L109
Norris, J. E., & Yong, D. 2019, ApJ, 879, 37
Onken, C. A., Wolf, C., Bessell, M. S., et al. 2024, PASA, 41, e061
Pace, A. B. 2024, arXiv:2411.07424
Perottoni, H. D., Placco, V. M., Almeida-Fernandes, F., et al. 2024, A&A, 691, A138
Placco, V. M., Almeida-Fernandes, F., Arentsen, A., et al. 2022, ApJS, 262, 8
Placco, V. M., Frebel, A., Beers, T. C., & Stancliffe, R. J. 2014, ApJ, 797, 21
Placco, V. M., Gupta, A. F., Almeida-Fernandes, F., et al. 2024, ApJ, 977, 12
Placco, V. M., Limberg, G., Chiti, A., et al. 2025, arXiv:2506.19163
Placco, V. M., Roederer, I. U., Lee, Y. S., et al. 2021a, ApJL, 912, L32
Placco, V. M., Sneden, C., Roederer, I. U., et al. 2021b, RNAAS, 5, 92
Popa, S. A., Hoppe, R., Bergemann, M., et al. 2023, A&A, 670, A25
Queiroz, A. B. A., Anders, F., Santiago, B. X., et al. 2018, MNRAS, 476, 2556
Roederer, I. U., Preston, G. W., Thompson, I. B., et al. 2014, AJ, 147, 136
Roederer, I. U., Sakari, C. M., Placco, V. M., et al. 2018, ApJ, 865, 129
Roman, N. G. 1950, ApJ, 112, 554
Rossi, S., Beers, T. C., & Sneden, C. 1999, in ASP Conf. Ser. 165, The Third Stromlo Symposium: The Galactic Halo, ed. B. K. Gibson, R. S. Axelrod, & M. E. Putman (San Francisco, CA: ASP), 264
Santiago, B. X., Brauer, D. E., Anders, F., et al. 2016, A&A, 585, A42

Schlafly, E. F., & Finkbeiner, D. P. 2011, ApJ, 737, 103
Schlegel, D. J., Finkbeiner, D. P., & Davis, M. 1998, ApJ, 500, 525
Skrutskie, M. F., Cutri, R. M., Stiening, R., et al. 2006, AJ, 131, 1163
Skúladóttir, Á., Salvadori, S., Amarsi, A. M., et al. 2021, ApJL, 915, L30
Sneden, C. A. 1973, PhD thesis, Univ. Texas, Austin
Sobeck, J. S., Kraft, R. P., Sneden, C., et al. 2011, AJ, 141, 175
Starkenburg, E., Aguado, D. S., Bonifacio, P., et al. 2018, MNRAS, 481, 3838
Starkenburg, E., Martin, N., Youakim, K., et al. 2017, MNRAS, 471, 2587
Suda, T., Katsuta, Y., Yamada, S., et al. 2008, PASJ, 60, 1159
Vasiliev, E. 2023, Galax, 11, 59
Vasiliev, E., Belokurov, V., & Erkal, D. 2021, MNRAS, 501, 2279
Venn, K. A., Starkenburg, E., Malo, L., Martin, N., & Laevens, B. P. M. 2017, MNRAS, 466, 3741
Wang, S., & Chen, X. 2019, ApJ, 877, 116
Whitten, D. D., Placco, V. M., Beers, T. C., et al. 2019, A&A, 622, A182
Whitten, D. D., Placco, V. M., Beers, T. C., et al. 2021, ApJ, 912, 147
Yao, Y., Ji, A. P., Koposov, S. E., & Limberg, G. 2024, MNRAS, 527, 10937
Yi, S., Demarque, P., Kim, Y.-C., et al. 2001, ApJS, 136, 417